Contrasting carbon dioxide removal potential and nutrient feedbacks of simulated ocean alkalinity enhancement and macroalgae afforestation

Lester Kwiatkowski, Manon Berger, Laurent Bopp, Stéphane Doléac, David Ho

ENVIRONMENTAL RESEARCH
LETTERS

LETTER • OPEN ACCESS

Contrasting carbon dioxide removal potential and nutrient feedbacks of simulated ocean alkalinity enhancement and macroalgae afforestation

To cite this article: Lester Kwiatkowski *et al* 2023 *Environ. Res. Lett.* **18** 124036

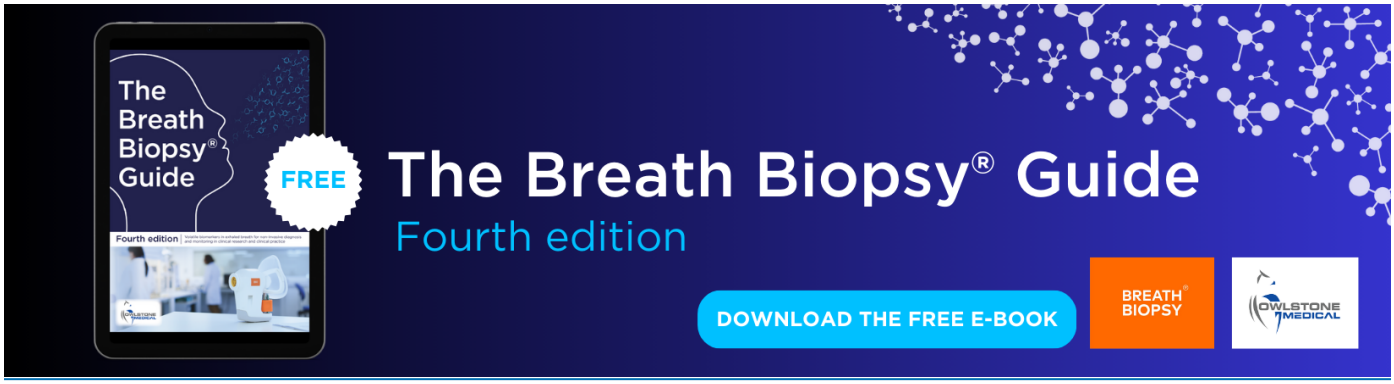

IOP Publishing Environ. Res. Lett. 18 (2023) 124036 https://doi.org/10.1088/1748-9326/ad08f9

ENVIRONMENTAL RESEARCH
LETTERS

OPEN ACCESS

RECEIVED
27 July 2023

REVISED
26 October 2023

ACCEPTED FOR PUBLICATION
1 November 2023

PUBLISHED
17 November 2023

LETTER

Contrasting carbon dioxide removal potential and nutrient feedbacks of simulated ocean alkalinity enhancement and macroalgae afforestation

Lester Kwiatkowski[1,*], **Manon Berger**[2], **Laurent Bopp**[2], **Stéphane Doléac**[1] **and David T Ho**[3,4]

[1] LOCEAN/IPSL, Sorbonne Université, CNRS, IRDMNHN, Paris 75005, France
[2] LMD/IPSL, Ecole Normale Supérieure/Université PSL, CNRS, Ecole Polytechnique, Sorbonne Université, Paris 75005, France
[3] Department of Oceanography, University of Hawai'i at Mānoa, Honolulu, HI 96822, United States of America
[4] [C]Worthy, Boulder, CO 80302, United States of America
[*] Author to whom any correspondence should be addressed.

E-mail: lester.morgan-kwiatkowski@locean.ipsl.fr

Keywords: carbon dioxide removal, ocean afforestation, ocean alkalinity enhancement, climate change

Supplementary material for this article is available online

Abstract

Alongside cuts to emissions, hundreds of gigatons of carbon dioxide removal (CDR) are likely to be required to limit global warming to below 1.5 °C or 2 °C this century. Ocean alkalinity enhancement (OAE) and macroalgae afforestation have received considerable attention within the portfolio of potential CDR options, but their efficacy and constraints remain uncertain. Here we compare the CDR potential and biogeochemical impacts of OAE and macroalgae afforestation in exclusive economic zones (EEZs) using a global high-resolution ocean biogeochemical model. Globally, our simulations indicate the CDR potential of OAE is more than seven times that of macroalgae afforestation for an equivalent mass of either dissolved olivine or harvested wet macroalgae biomass. This difference is predominately attributable to the respective alkalinity content of olivine and carbon content of wet macroalgae biomass. Accounting for potential nutrient impacts on phytoplankton production increases this disparity between the CDR efficiency of OAE and afforestation, and in both cases can result in regions of negative CDR. EEZs with higher CDR in response to OAE consistently exhibit higher CDR in response to macroalgae afforestation. However, nutrient feedbacks are shown to have different EEZ-specific impacts on phytoplankton net primary production. Our simulations indicate that ∼62% of the CDR flux associated with OAE occurs in the EEZ application regions, decreasing to ∼54% if olivine contains iron and silicate and ∼45% for macroalgae afforestation. This suggests that monitoring, reporting, and verification may be problematic for both techniques, as might the allocation of credits toward nationally determined contributions.

1. Introduction

Emissions scenarios consistent with a 50% probability of keeping global warming below 1.5 °C in 2100 require cumulative 21st century novel carbon dioxide removal (CDR) of 24–860 Gt CO_2 (Smith *et al* 2023). Even scenarios consistent with keeping global warming below 2 °C (67% probability) require cumulative novel CDR of 160–660 Gt CO_2. Two ocean-based novel CDR methods that may have the potential to remove 0.1 to >1 Gt CO_2 yr^{-1} (National Academies of Sciences, Engineering, and Medicine 2022) are macroalgae afforestation and ocean alkalinity enhancement (OAE).

Macroalgae, or seaweed, afforestation involves the cultivation of marine seaweeds that convert dissolved inorganic carbon (DIC) into organic carbon during net primary production (NPP), which lowers the surface ocean partial pressure of CO_2 (pCO_2) and increases the ocean-atmosphere pCO_2 gradient,

increasing ocean carbon uptake. The resulting macroalgae biomass can then either be harvested or conveyed deep enough in the water column so that remineralized CO_2 remains out of contact with the atmosphere on multi-centennial timescales (Siegel *et al* 2021).

Assessments of the CDR potential of macroalgae have relied on upscaled experimental studies (Froehlich *et al* 2019, Duarte *et al* 2022), natural analogues (Bach *et al* 2021), idealized ocean biogeochemical model simulations (Orr and Sarmiento 1992, Berger *et al* 2023), and simulations incorporating explicit macroalgae representations (Frieder *et al* 2022, Wu *et al* 2023). Such simulations have demonstrated that CDR is typically less than 70% of macroalgae carbon fixation and macroalgal consumption of nutrients can limit regional efficacy through phytoplankton NPP feedbacks (Berger *et al* 2023).

OAE, first proposed by Kheshgi (1995), promotes the conversion of dissolved CO_2 into bicarbonate and carbonate ions, thereby reducing ocean pCO_2. If this occurs in surface waters, the enhanced ocean-atmosphere pCO_2 gradient increases the flux of atmospheric CO_2 into the ocean. Proposed methods of OAE include the dissolution of minerals of silicate (e.g. olivine), carbonate (e.g. calcite), and alkaline-rich industrial waste products, as well as electrochemical generation of NaOH.

Multiple studies have used a variety of ocean biogeochemical and Earth system models to simulate the global CDR potential of OAE (Ilyina *et al* 2013, Köhler *et al* 2013, Keller *et al* 2014, González and Ilyina 2016, Hauck *et al* 2016, Lenton *et al* 2018). Region-specific simulations assessing the potential for CDR and acidification mitigation have also been performed (Feng *et al* 2016, 2017, Burt *et al* 2021, Butenschön *et al* 2021, Mongin *et al* 2021, He and Tyka 2023, Wang *et al* 2023). However, with few exceptions (e.g. Hauck *et al* 2016), studies typically assume no co-delivery of nutrients during alkalinity enhancement. Therefore, these studies have not examined the effect of OAE on phytoplankton NPP, which could affect the projected CDR.

Frameworks such as the CDR intercomparison project (Keller *et al* 2018) have been established to compare the efficacy of OAE and land-based afforestation scenarios. However, a global CDR comparison of OAE and macroalgae afforestation within the same model has, to the best of our knowledge, not yet been performed. A major uncertainty in both OAE and macroalgae afforestation deployments is how the biogeochemical cycling of elements other than carbon is affected, the impacts on calcification (Bach *et al* 2021), and the repercussions for CDR (National Academies of Sciences, Engineering, and Medicine 2022) and marine ecosystems (e.g. Levin *et al* 2023).

Here we compare the CDR potential and biogeochemical impacts of OAE and macroalgae afforestation in the exclusive economic zones (EEZs) of coastal countries using a global high-resolution ocean biogeochemical model forced with an atmospheric reanalysis over the 2006–2010 period. Our idealized simulations assume that an equivalent mass of alkalinity-rich mineral (olivine) or wet macroalgae biomass is respectively either dissolved or harvested from the global ocean. We further assess how CDR efficacy and biogeochemical impacts may be influenced by potential nutrient feedbacks on phytoplankton productivity in both deployments.

2. Methods

All simulations were performed with the Nucleus for European Modelling of the Ocean (NEMO)-Pelagic Interaction Scheme for Carbon and Ecosystem Studies (PISCES) ocean biogeochemical model using version 3.6 of NEMO (Madec *et al* 2019), version 3 of the Louvain-La-Neuve sea Ice Model (Rousset *et al* 2015) and version 2 of the PISCES ocean biogeochemical model (Aumont *et al* 2015). The model was run in a high-resolution eORCA025 global configuration, with a nominal horizontal resolution of 0.25°, deemed adequate to represent EEZ boundaries. This configuration includes 75 vertical depth levels, 7 of which are in the upper 10 m of the water column (where alkalinity addition is simulated) and 23 of which are in the upper 100 m (where macroalgae production is simulated).

Ocean biogeochemistry, central to simulations of marine CDR, is represented by PISCES (Aumont *et al* 2015). PISCES is a relatively complex global ocean biogeochemical model well-suited to climate applications (Boucher *et al* 2020, Kwiatkowski *et al* 2020, Séférian *et al* 2020), ocean acidification projections (Orr *et al* 2022, Kwiatkowski *et al* 2023b), and has been previously used in CDR simulations of both ocean iron fertilization (Aumont and Bopp 2006) and macroalgae afforestation (Berger *et al* 2023). It represents the cycles of organic and inorganic ocean carbon, total alkalinity, oxygen, and essential marine nutrients (N, P, Si, and Fe). It includes two phytoplankton functional types (diatoms and nanophytoplankton) and two zooplankton size classes, alongside two particulate organic matter size classes, particulate inorganic matter (calcite) and dissolved organic matter. Pelagic calcification is parameterized as a function of NPP and is insensitive to the calcite saturation state (Planchat *et al* 2023). Air–sea CO_2 fluxes, including those associated with CDR simulations, follow Ocean Model Intercomparison Project protocols (Orr *et al* 2017), with gas exchange dependent on the air–sea partial pressure gradient and a parameterization of the instantaneous gas transfer velocity that depends on 10 m atmospheric wind speed (Wanninkhof 1992, Ho *et al* 2006).

The NEMO-PISCES historical control simulation, against which all CDR simulations were assessed, was initialized from a combination of

data-based climatologies and a coarser resolution NEMO-PISCES simulation of ocean anthropogenic carbon concentrations (Terhaar *et al* 2019). The control simulation was subsequently performed between 1958 and 2016 using atmospheric reanalysis forcing (Drakkar forcing set 5.2; Dussin *et al* 2016) and annually resolved historic CO_2 concentrations. The globally integrated total ocean carbon flux and its spatial distribution in the control simulation are in reasonable agreement with data-based estimates as is the integrated anthropogenic carbon flux (figures S1 and S2). All CDR simulations were performed over the years 2006–2010 using the same model configuration and atmospheric forcing as the control. Consequently, all simulations experience the same climate variability although the impact of that variability on CDR simulations may differ.

2.1. CDR simulations

CDR is computed as the change in total air–sea CO_2 flux in macroalgae afforestation and OAE simulations relative to the coincident 2006–2010 historical control simulation. As most of the ocean surface exhibits net uptake of atmospheric CO_2 in the control simulation (figure S2b), positive CDR will typically reflect a local increase in ocean CO_2 uptake. However, it can also reflect a reduction in local CO_2 outgassing that may, or may not, be accompanied by a switch to net uptake. Similarly, negative CDR can represent either an enhancement in local CO_2 outgassing or a decline in CO_2 uptake that may, or may not, result in a switch to net outgassing.

2.2. Macroalgae simulations

The two macroalgae afforestation simulations used are previously described in detail in Berger *et al* (2023). Both simulations represent idealized macroalgae production as a permanent loss of DIC. This permanent loss of ocean DIC is analogous to macroalgae production followed by complete biomass harvesting with sequestration external to the ocean via unspecified means and at no carbon cost. The simulations neither represent the production of macroalgae organic carbon nor any export and subsequent remineralization of such macroalgae organic carbon in the deep ocean. Moreover, in both simulations ocean circulation and hydrodynamics were unaffected by macroalgae production.

The first simulation, hereafter referred to as *Macro* (Geo in Berger *et al* 2023) prescribes a global macroalgae production rate of 0.5 PgC yr^{-1} that is equally distributed over the upper 100 m of all EEZs currently free of seasonal sea ice, with a mean sea surface temperature between 0 °C and 35 °C, and an average nitrate to phosphate ratio between 4:1 and 80:1. EEZ boundaries are defined using the Sea Around Us data product (www.seaaroundus.org) that subdivides the EEZs of 198 coastal states, including territorial seas and overseas territories, into a total of 280 EEZ regions. The second simulation, hereafter referred to as *Macro-N* (BioGeo in Berger *et al* 2023) is identical to *Macro* but in addition to DIC consumption, nitrate, and phosphate are also consumed at a fixed C:N:P ratio of 800:49:1 with production only occurring if nitrate and phosphate concentrations are sufficient. This results in realized global macroalgae production <0.5 PgC yr^{-1} (0.37 PgC yr^{-1} in 2010). Although both simulations resolve the planktonic community and its impact on the carbon cycle, planktonic processes are unaffected by macroalgae production in the *Macro* simulation. In contrast in the *Macro-N* simulation, macroalgae nutrient consumption has the potential to affect phytoplankton production, impacting zooplankton, the production of plankton-derived organic and inorganic matter, and air–sea carbon fluxes.

2.3. OAE simulations

Idealized OAE simulations were designed to compare CDR potential to that of macroalgae afforestation based on equivalent harvested or added mass. The 0.5 PgC yr^{-1} of prescribed global macroalgal production in the *Macro* simulation represents 11.7 Pg yr^{-1} (11.7 Gt yr^{-1}) of harvested wet weight assuming that 29.8% of dry macroalgal weight is carbon and a dry-weight to wet-weight ratio of 1:7 (Berger *et al* 2023). An equivalent 11.7 Pg yr^{-1} (11.7 Gt yr^{-1}) of olivine addition represents 0.32 Pmol yr^{-1} of alkalinity addition, given an assumed molar mass of olivine of 147 g mol^{-1} and 4 mol of alkalinity per mol of olivine. This alkalinity addition is higher than previous global OAE simulations of 0.1–0.25 Pmol yr^{-1} (Hauck *et al* 2016, Keller *et al* 2018, Burt *et al* 2021).

Two OAE simulations were performed. The first, hereafter referred to as *Alk*, enhances global total alkalinity by 0.32 Pmol yr^{-1}, with alkalinity addition occurring homogeneously and continuously in the upper 10.7 m of EEZs without present-day seasonal sea ice. This represents a volume-specific alkalinity addition rate of 3×10^{-4} mol l^{-1} yr^{-1} in the regions of OAE. The second simulation, hereafter referred to as *Alk + N*, is similar to OAE but alongside the addition of 0.32 Pmol yr^{-1} of alkalinity, silicate, and iron, which naturally occur in olivine, are additionally supplied. Assuming olivine has a Mg:Fe molar ratio of 9:1 and following Hauck *et al* (2016), dissolved silicate is increased by 1 mol and dissolved iron by 0.2 mol per mol of dissolved olivine with only 1% of the added iron considered bioavailable. The total amount of added dissolved silicate and iron is therefore 0.08 Pmol yr^{-1} and 0.16 Tmol yr^{-1}, respectively. Due to the absence of nitrate-to-phosphate ratio constraints, the EEZ regions of alkalinity enhancement are more extensive than those of macroalgae afforestation, particularly in the low latitudes. EEZ-specific comparisons therefore only include EEZs which have both CDR interventions simulated throughout their extent.

The scale of both the OAE and macroalgae afforestation simulations is likely highly unrealistic in any real-world implementation yet like previous studies (e.g. Orr and Sarmiento 1992, Köhler *et al* 2013, Hauck *et al* 2016, Berger *et al* 2023) provides insights into the physical and biogeochemical limits of these proposals. For context, current global maritime shipping transports 11 Gt yr^{-1} of goods (UNCTAD 2022), and the current global marine fish catch is 80 Mt yr^{-1} (FAO 2022). Therefore, the mass of harvested macroalgae and olivine addition in our simulations (11.7 Gt yr^{-1}) is ∼150 times that of the global marine fish catch and roughly equivalent to the total tonnage of global maritime shipping.

3. Results

3.1. CDR, phytoplankton production, and ocean carbon export

All simulations resulted in enhanced global ocean carbon uptake relative to the control simulation (i.e. CDR), with CDR increasing over the simulation period and near-stable in the final simulation year of 2010 (figure 1(a), table 1). The magnitude of CDR, however, differed substantially across simulations. Global scale CDR in the *Alk* simulation was 2.95 Pg C yr^{-1} (10.8 Pg CO_2 yr^{-1}) in 2010 (0.92 Pg of CO_2 per Pg of olivine or 0.76 mol of CO_2 per mol of alkalinity). In the *Alk* + *N* simulation, which accounted for additional inputs of iron and silicate, this increased to 4.16 Pg C yr^{-1} (15.3 Pg CO_2 yr^{-1}) in 2010 (1.32 Pg of CO_2 per Pg of added olivine or 1.08 mol of CO_2 per mol of alkalinity). In contrast in the *Macro* simulation, CDR was 0.39 Pg C yr^{-1} (1.43 Pg CO_2 yr^{-1}) in 2010 (0.12 Pg of CO_2 per Pg of harvested wet biomass or 0.79 mol CO_2 per mol of carbon harvested). This CDR decreased in the *Macro-N* simulation that accounted for nutrient limitation and uptake to 0.21 Pg C yr^{-1} (0.77 Pg CO_2 yr^{-1}) in 2010 (0.09 Pg CO_2 per Pg of harvested wet biomass or 0.58 mol CO_2 per mol of carbon harvested).

Global phytoplankton NPP and particulate carbon export at 100 m (C_{exp}) were effectively unchanged in the *OAE* and *Macro* simulations (figures 1(c) and (e)). This is expected given that planktonic primary production and calcification are unaffected by the concentrations of DIC and alkalinity in PISCES and these are the only prognostic variables that are directly impacted in these simulations. In the *Alk* + *N* simulation the addition of iron and silicate resulted in an initial increase in NPP of ∼10 Pg C yr^{-1} which subsequently declined, to 4.0 Pg C yr^{-1} in the final simulation year, albeit with large seasonal and interannual variability. This NPP enhancement was associated with a coincident ∼2 Pg C yr^{-1} increase in the carbon export at 100 m. The opposite however occurred in the *Macro-N* simulation, with macroalgal consumption of nitrate and phosphate suppressing NPP by 1.2 Pg C yr^{-1} and decreasing carbon export by 0.23 Pg C yr^{-1} in the final year of the simulation.

3.2. Internal and external EEZ impacts

A general decline in the fraction of global CDR that occurred within EEZ intervention regions is seen across all simulations (figure 1(b)). There are however differences in the rate of decline. At the start of simulations in 2006, ∼90% of CDR occurred within the respective EEZ intervention areas. However, in 2010 this declined to 62% in the *Alk* simulation, 54% in *Alk* + *N* and ∼45% in *Macro* and *Macro-N*. Similar declines are seen in the fraction of NPP and C_{exp} anomalies that occur in EEZ regions in the *Alk* + *N* and *Macro-N* simulations (figures 1(d) and (f)). Specifically, in 2010, 47% of the NPP reduction and 59% of the C_{exp} reduction in the *Macro-N* simulation occurred in EEZs with the rest occurring in non-EEZ waters. While in the *Alk* + *N* simulation, only 22% of NPP and 37% of C_{exp} enhancement occurred in EEZs in 2010.

3.3. Regions of negative CDR when nutrients are simulated

In the *Alk* and *Macro* simulations, the mean CDR rate over the 5 simulation years was highest in the respective EEZ regions of alkalinity addition and DIC consumption (figures 2(a) and (c)). However, in non-EEZ waters, CDR was still either positive, indicative of enhanced ocean carbon uptake, or near zero. In contrast, in the *Alk* + *N* and *Macro-N* simulations, which respectively consider olivine-associated supply of nutrients and macroalgae-associated consumption of nutrients, there were regions that exhibit negative CDR (figures 2(b) and (d)). This negative CDR, or reduction in net ocean carbon uptake relative to the control, was particularly apparent in non-EEZ regions of the Pacific and Atlantic Southern subtropical gyres in the *Alk* + *N* simulation. Negative CDR was much lower in magnitude in the *Macro-N* simulation, occurring both within and outside EEZ afforestation regions of the Western equatorial Pacific and Indian Ocean.

3.4. CDR efficiencies across EEZs

There is a strong linear relationship between EEZ-specific CDR in the *Alk* and *Macro* simulations with a regression slope of $0.15 + 0.002$ ($p < 0.001$, $R^2 = 0.99$, figure 3). This is indicative of typically 7.5 times the CDR in each EEZ for a given mass of olivine addition than from the same mass of wet macroalgae biomass harvested. All EEZs exhibited higher CDR in *Alk* than *Macro*, with the vast majority exhibiting CDR below 0.2 Pg of C per Pg of olivine in *Alk* and below 0.025 Pg of C per Pg of harvested wet macroalgae in *Macro*. A small number of EEZs exhibited CDR of 0.2–0.6 Pg of C per Pg of olivine in *Alk* and between 0.03–0.07 Pg of C per Pg of harvested wet macroalgae biomass in *Macro*.

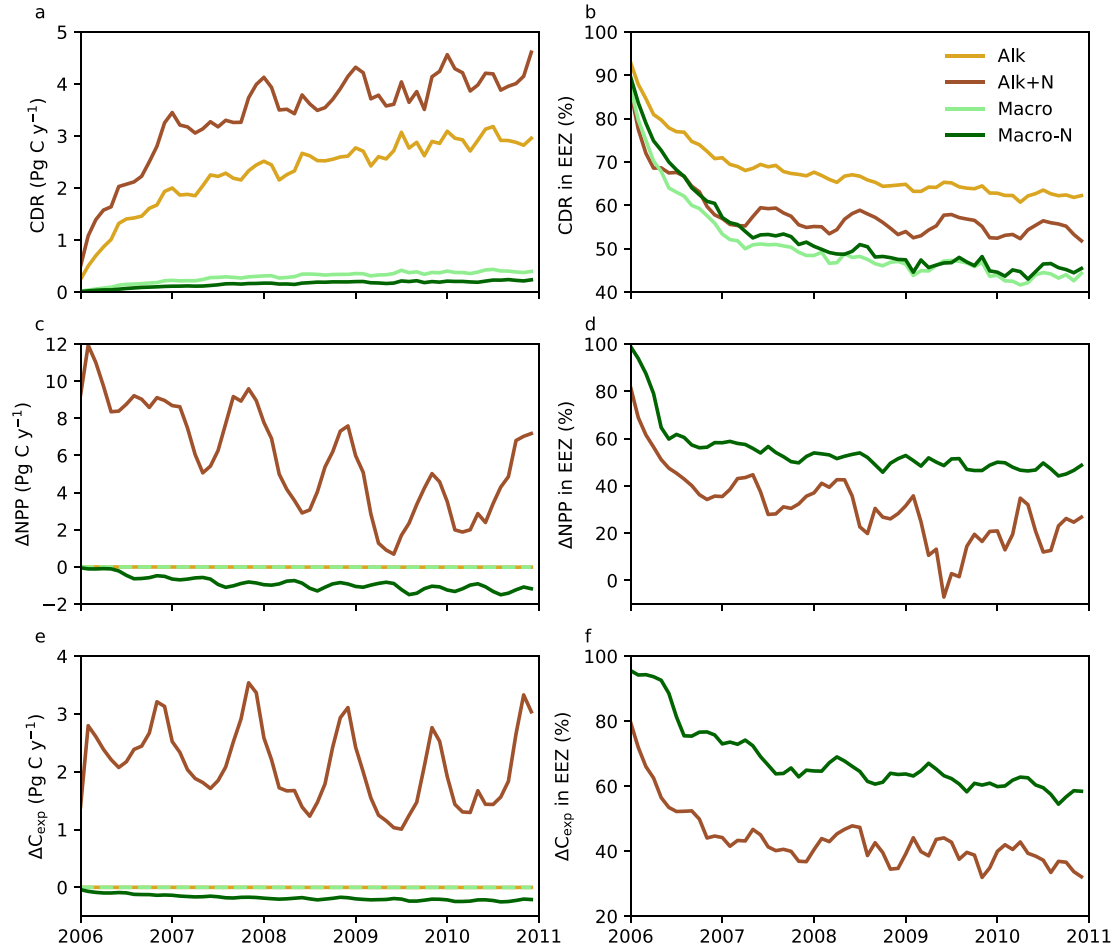

Figure 1. Global ocean carbon dioxide removal and impacts on phytoplankton net primary production and carbon export flux. The global (a), carbon dioxide removal (CDR), (c), phytoplankton net primary production anomaly (ΔNPP) and (e), carbon export flux at 100 m anomaly (ΔC_{exp}), and (b), (d), (f), the fraction of each that occurs within the respective EEZ area of alkalinity enhancement or afforestation. All values are calculated relative to the coincident control simulation, with CDR equivalent to the change in air–sea carbon flux (ΔCO_2 flux).

Table 1. The simulated global ocean carbon uptake (C_{flx}), integrated net primary production (NPP) and carbon export at 100 m (C_{exp}) in the control simulation, and the anomaly in the different CDR simulations.

			Anomaly in CDR simulation (PgC yr^{-1})			
	Year (s)	Control (PgC yr^{-1})	*Alk*	*Alk* + *N*	*Macro*	*Macro-N*
C_{flx}	2006	2.44	1.78	1.93	0.12	0.06
	2010	2.59	2.95	4.16	0.40	0.21
	2006–2010	2.53	2.29	3.41	0.29	0.16
NPP	2006	49.4	—	9.36	—	−0.33
	2010	50.2	—	4.02	—	−1.20
	2006–2010	49.8	—	5.91	—	−0.85
C_{exp}	2006	8.25	—	2.46	—	−0.10
	2010	8.41	—	1.91	—	−0.23
	2006–2010	8.30	—	2.09	—	−0.18

In contrast, the impact of accounting for nutrient supply and consumption on EEZ-specific CDR differed between the *Alk* + *N* and *Macro-N* simulations (figure 3). The EEZs that exhibited the greatest increases in CDR in *Alk* + *N* compared to *Alk* generally exhibited similar CDR in *Macro* and *Macro-N*, while EEZs that exhibited the greatest reductions in CDR in *Macro-N* relative to *Macro* generally exhibited similar CDR in *Alk* and *Alk* + *N*. EEZ-specific CDR anomalies in the simulations that accounted for additional nutrient feedbacks were typically less than ±5% relative to the respective *Alk* and *Macro* simulations but in a small number of EEZs were +20% to −40%.

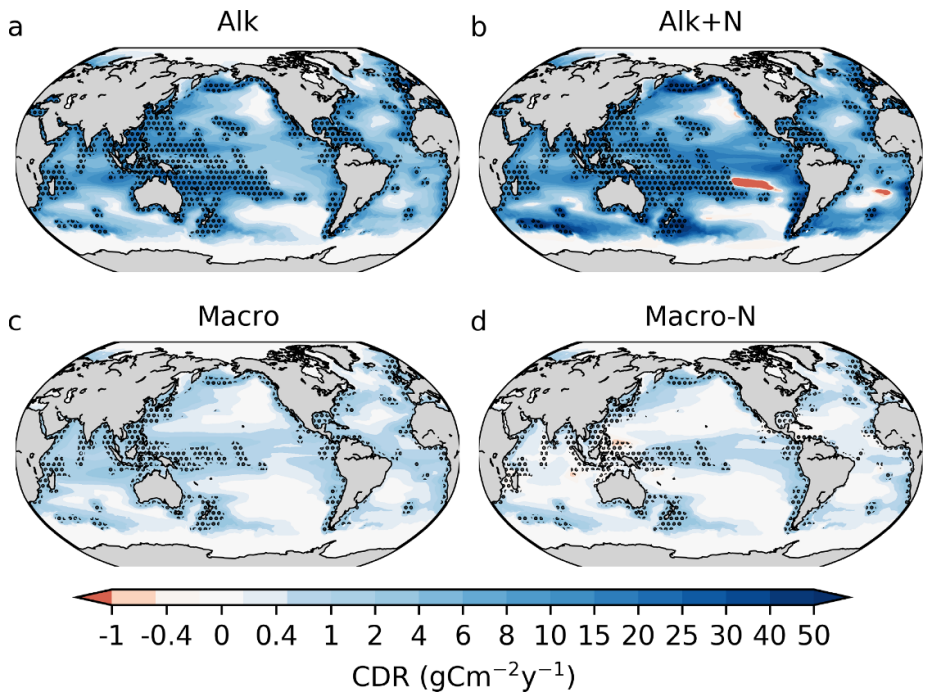

Figure 2. The spatial distribution of carbon dioxide removal associated with ocean alkalinity enhancement and afforestation simulations. The 2006–2010 mean CDR associated with (a), OAE, (b), OAE with nutrient co-delivery, (c), macroalgae afforestation, and (d), macroalgae afforestation with associated nutrient consumption/limitation. CDR is the change in air–sea carbon flux in each simulation relative to coincident 2006–2010 control simulation. Stippled areas correspond to the respective areas of OAE and macroalgal cultivation.

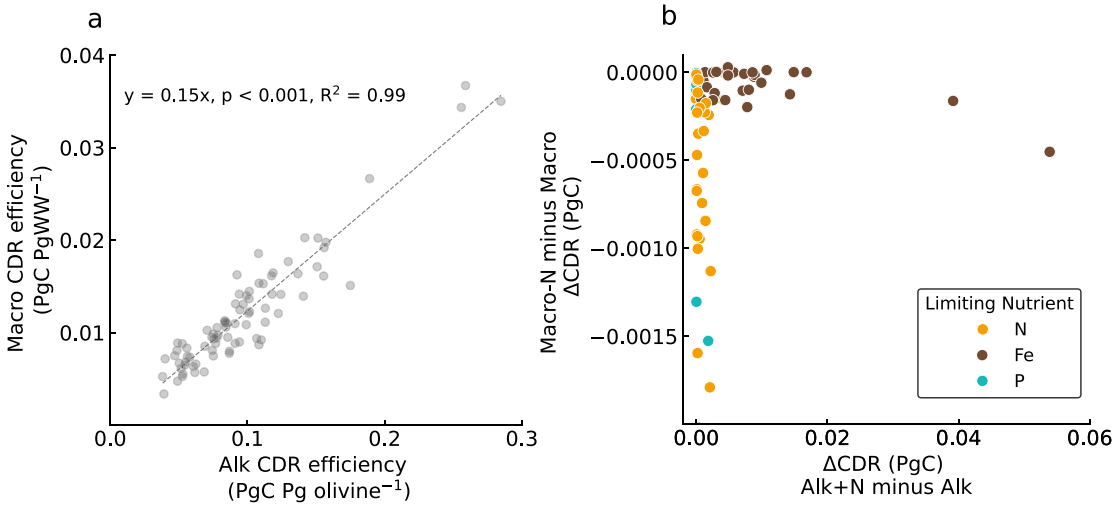

Figure 3. The EEZ-specific CDR efficiency of OAE and macroalgae afforestation and the impact of nutrient feedbacks. (a) The 2006–2010 mean EEZ-specific CDR per unit of olivine addition (*Alk*) and harvested macroalgae wet weight (*Macro*) assuming no associated nutrient delivery or consumption. (b) The EEZ-specific change in CDR when olivine iron and silicate supply is simulated (*Alk* + *N* minus *Alk*) and macroalgae associated nitrate and phosphate consumption is simulated (*Macro-N* minus *Macro*). The most limiting nutrient for nanophytoplankton primary production in the control simulation is designated for each EEZ (orange = nitrogen, brown = iron, and blue = phosphate). Of the 280 EEZ regions, only those that have both OAE and macroalgae afforestation throughout their extent are shown.

4. Discussion

4.1. Higher CDR with OAE than macroalgal afforestation

The general finding of approximately 7–10-fold higher global CDR with OAE than macroalgae afforestation for an identical mass of added olivine or harvested wet biomass is largely attributable to the respective alkalinity content of olivine and carbon content of wet macroalgae biomass. The mean macroalgae dry-weight carbon content of 29.8% and dry-weight to wet-weight ratio of 1:7 identified in the literature review of Berger *et al* (2023) equates the 0.5 Pg C yr^{-1} or 0.042 Pmol C of imposed global

macroalgal production in the *Macro* simulation to 11.7 Pg yr^{-1} of harvested wet weight; while an equivalent 11.7 Pg yr^{-1} of olivine addition represents 0.32 Pmol yr^{-1} of alkalinity addition. In the final simulation year, global CDR in *Alk* was 7.6 times that of *Macro*, similar to the molar ratio of added alkalinity to removed DIC, with 0.76 mol of CDR per mol of alkalinity enhancement in *Alk* and 0.79 mol of CDR per mol of DIC removal in *Macro*. This similarity in CDR per mol of either added alkalinity or removed DIC occurs despite differences in the EEZ masks of alkalinity enhancement and DIC removal and must be a consequence of various compensating factors. The physical and geochemical constraints that limit global CDR efficiency to 0.79 mol C per mol of DIC removal in the *Macro* simulation are discussed by Berger *et al* (2023), and in broad agreement with comparable model studies (e.g. Orr and Sarmiento 1992, Wu *et al* 2023).

Other factors being equal, the molar change in equilibrated surface ocean DIC is ∼0.81–0.84 times the molar change in alkalinity under present-day ocean carbonate chemistry conditions (Planchat *et al* 2023). This constrains global scale CDR to a maximum of ∼0.81–0.84 mol of C per mol of alkalinity enhancement. In the *Alk* simulation this limit is not attained, likely due to the circulation and mixing of alkalinity into the ocean interior prior to full equilibration with the atmosphere. Comparable OAE simulations in other global ocean circulation and biogeochemical models have similarly demonstrated this (Burt *et al* 2021, He and Tyka 2023). Nonetheless, given this additional constraint, the similarity between the molar efficiencies of the *Alk* and *Macro* simulations likely also reflects alkalinity enhancement occurring closer to the ocean surface (upper 10 m) than imposed macroalgae production (upper 100 m) in our simulations.

Accounting for the impacts of olivine-associated supply of iron and silicate, and macroalgae-associated consumption of nitrate and phosphate enhances the disparity in global scale CDR between OAE and afforestation simulations (figure 1). Coincident fertilization in the *Alk* + *N* simulation enhances CDR to 1.08 mol C per mol of alkalinity (i.e. above the maximum attainable CDR of alkalinity enhancement alone). Such a fertilization effect typically declines over time due to the loss of other limiting nutrients from the upper ocean (Aumont and Bopp 2006, Hauck *et al* 2016). In contrast, macroalgae nitrate and phosphate limitation and uptake in the *Macro-N* simulation reduce CDR to 0.58 mol C per mol of carbon harvested. This disparity in CDR per mol of alkalinity added or DIC removed is a consequence of enhanced phytoplankton NPP in regions of iron and silicate limitation in *Alk* + *N* and suppressed NPP in regions of nitrate and phosphate limitation in *Macro-N*. An additional contributing factor is a deepening of maximal macroalgae production due to typically greater nitrate and phosphate limitation in surface waters in the *Macro-N* simulation (Berger *et al* 2023).

4.2. Regions of negative CDR when nutrient feedbacks are simulated

The appearance of regions of negative CDR occurs in the *Alk* + *N* and *Macro-N* simulations that respectively represent the olivine-associated supply of iron and silicate and macroalgae-associated consumption of nitrate and phosphate. These negative CDR regions, broadly absent in the *Alk* and *Macro* simulations, are a consequence of nutrient feedbacks on phytoplankton NPP, zooplankton grazing, particulate ocean carbon export, and the subsequent impact on the air–sea carbon flux. As discussed in Berger *et al* (2023), in regions of phytoplankton nitrate or phosphate limitation, the macroalgal consumption of nitrate and phosphate, both locally or in waters transported into the region, will reduce phytoplankton NPP. Depending on differences in the relative magnitudes and vertical profiles of macroalgae production and phytoplankton NPP suppression, this can in rare cases enhance surface ocean pCO_2 and reduce the local ocean carbon sink relative to the control, as in the West Pacific in the *Macro-N* simulation.

Similarly, in the *Alk* + *N* simulation, although global phytoplankton NPP is enhanced by the supply of iron and silicate, there are regions, such as in the tropical Pacific, that exhibit declines in NPP and negative CDR. This occurs when the alleviation of phytoplankton silicate and iron limitation in one region increases nitrate and phosphate consumption, limiting the supply of these nutrients to adjacent regions where they would otherwise have been utilized by phytoplankton (Aumont and Bopp 2006). Nutrient feedbacks of CDR technologies on phytoplankton, either via mineral co-delivery or macroalgae consumption can therefore result in regions of negative CDR outside the EEZ area of application. This highlights the need for extensive evaluation of marine CDR technologies during development and widespread monitoring, reporting, and verification (MRV) throughout implementation.

4.3. Differences in the EEZ CDR fraction

The general decrease in the fraction of CDR that occurs within EEZ regions over time (figure 1(b)) can be explained by the circulation and mixing of water masses that transport DIC, alkalinity, and nutrient anomalies out of EEZs and result in generally enhanced ocean carbon uptake outside these regions (Jones *et al* 2014, Berger *et al* 2023). The greater decline in the EEZ CDR fraction in the macroalgae afforestation simulations can be partially explained by differences in the vertical profiles of imposed DIC, alkalinity, and nutrient anomalies. In the OAE simulations, initial enhancement of alkalinity and dissolved nutrients occurs in the upper 10 m while in the afforestation simulations, macroalgae-associated

DIC and nutrient consumption is either imposed or permissible up to 100 m. Consequently, a greater proportion of water masses in the OAE simulations can equilibrate with the atmosphere and enhance ocean carbon uptake prior to being transported out of the EEZ regions. The reduced fraction of CDR that occurs in EEZs in the *Alk* + *N* simulation compared to the *Alk* simulation is a consequence of surplus iron and silicate transport from EEZs. This fertilization generally enhances NPP, carbon export, and therefore ocean carbon uptake in non-EEZ regions (figures 1(d) and (f)).

The higher fraction of CDR that occurs within EEZ regions in the OAE simulations than in the afforestation simulations may be indicative of easier MRV in any real-world implementation. However, this potential advantage is diminished when olivine nutrient supply and feedbacks are considered. Moreover, within a year of each simulation, greater than 30% of CDR occurs outside EEZs in some cases hundreds of kilometers away, posing a substantial MRV challenge for both OAE and afforestation.

4.4. OAE and afforestation CDR across EEZs

The linear relationship between EEZ-specific CDR across the *Alk* and *Macro* simulations (figure 3(a)) is indicative of physicochemical dynamics being the principal driver of CDR efficiency across EEZs when nutrient feedbacks are not simulated. This linear relationship is unsurprising given that imposed anomalies in DIC and alkalinity are the only difference between these simulations and they have identical atmospheric conditions, ocean temperatures, circulation and EEZ water residence times.

The finding that the EEZs most impacted by olivine nutrient co-delivery are generally different from those impacted by macroalgae nutrient consumption is reflective of differences in the nutrients supplied/consumed and spatially variable nutrient constraints on phytoplankton NPP. In PISCES, as in most ocean biogeochemical models, nutrient limitation of phytoplankton is set by the most limiting nutrient with respect to nitrogen (NO_3 + NH_4), phosphate, iron, and silicate (Aumont *et al* 2015). The EEZs that exhibit the greatest CDR increases in *Alk* + *N* relative to *Alk* are predominately iron or silicate limited in the control simulation (figures 3(b) and S3) and these are the nutrients enhanced. In contrast, the EEZs with the greatest CDR reductions in *Macro-N* relative to *Macro* are predominately nitrogen and phosphate limited in the control simulation and these are the only nutrients macroalgae are assumed to be limited by and consumed in the *Macro-N* simulation. Emerging evidence of macroalgae iron requirements (Paine *et al* 2023) suggests this may be an oversimplification.

4.5. Caveats and future developments

The much higher CDR in OAE simulations than in afforestation simulations is contingent on multiple assumptions. (i) We assumed that all macroalgae were harvested as wet weight, but if biomass could be dried prior to harvest, up to seven-times as much carbon could be harvested for the same mass. (ii) We assumed that all olivine instantaneously dissolved in the upper 10 m. In reality, a fraction of the olivine may dissolve in deeper waters, or not at all, reducing OAE-based CDR. (iii) In our idealized simulations, we take no account of either post-harvest sequestration of macroalgae carbon or pre-deposition mining and processing of olivine. The inclusion of these processes within a full life-cycle assessment of each CDR intervention, alongside the evaluation of other alkalinity-rich minerals is critical to a thorough comparison.

Additionally, the use of a concentration-driven ocean biogeochemical model neglects the feedback that enhanced air–sea carbon flux has on atmospheric CO_2 and interactions with terrestrial carbon uptake. Such feedbacks reduce the mole fraction of atmospheric CO_2 and thereby the effectiveness of ocean CDR interventions (Oschlies 2009, Oschlies *et al* 2010, Lenton *et al* 2018). For this reason, our simulated CDR for both afforestation and OAE interventions should be considered overestimated. Although this should not influence the comparison of the interventions, it highlights the value of complimentary emissions-driven simulations that account for atmospheric and terrestrial carbon cycle feedbacks.

Our CDR simulations result in net global increases in aragonite saturation state (Ω_{arag}) and pH (figures S3, S6 and S7) but Ω_{arag} values typically remain below 6 and are therefore unlikely to result in potentially problematic $CaCO_3$ precipitation. Given that CDR and impacts on NPP and carbon export do not reach steady state in our 5 year simulations, longer duration simulations are desirable. However, model configurations capable of resolving coastal EEZs are computationally intensive. As such, configurations such as those presented here need to be used alongside lower resolution and simplified global configurations, as well as regional models, when determining centennial-scale impacts of CDR interventions. From the idealized global simulations presented here, we are unable to explicitly identify how CDR interventions in different EEZs interact. EEZ-specific CDR efficiencies should therefore also be estimated in simulations where interventions occur in individual EEZs.

The NEMO-PISCES high-resolution global ocean biogeochemical model configuration utilized here represents an additional testbed for the assessment of ocean CDR technologies. Within the context of

more advanced OAE and afforestation simulations, implementations that account for impacts on albedo, turbidity, light attenuation, heavy metal toxicity, and organic matter recycling pathways represent research priorities.

5. Conclusion

Idealized simulations of OAE and macroalgae afforestation in EEZs indicate the global CDR potential of OAE is more than seven times greater than that of afforestation for an equivalent mass of either dissolved olivine or harvested wet macroalgae biomass. The comparative inefficiency of afforestation is principally driven by the respective alkalinity content of olivine and carbon content of wet macroalgae biomass and is enhanced when the phytoplankton NPP feedbacks of olivine nutrient co-delivery and macroalgae nutrient consumption are simulated. EEZs that exhibit higher CDR under OAE consistently exhibit higher CDR under afforestation, indicative of EEZ-specific physicochemical ocean dynamics being the principal driver of local CDR efficiency. However, due to EEZ-specific nutrient constraints on phytoplankton NPP, the impact of olivine-associated nutrient co-delivery and macroalgae nutrient consumption differs across EEZs. After 5 years, only ∼54% of the CDR associated with OAE and ∼45% of that associated with macroalgae afforestation occurs within the regions of intervention. This is a consequence of the timescales of air–sea equilibration and the water residence times in EEZs, and is likely to present a challenge to MRV and the allocation of credits toward nationally determined contributions.

Data availability statement

The data that support the findings of this study are openly available at the following URL/DOI: https://doi.org/10.5281/zenodo.8189997 (Kwiatkowski *et al* 2023a).

Acknowledgments

The authors thank the IPSL modeling group for the software infrastructure, which facilitated model simulations and analysis. Authors received funding from the ENS-Chanel research chair. Simulations were carried out with computational resources from TGCC through a GENCI/DARI grant (gen0040). Model output was analysed on the IPSL Prodiguer-Ciclad cluster, a facility supported by CNRS, Sorbonne Université, and Labex L-IPSL, the latter being funded by ANR (Grant ANR-10-LABX-0018) and European FP7 IS-ENES2 project (Grant 312979).

ORCID iDs

Lester Kwiatkowski https://orcid.org/0000-0002-6769-5957
Manon Berger https://orcid.org/0000-0002-6519-5393

References

Aumont O and Bopp L 2006 Globalizing results from ocean in situ iron fertilization studies *Glob. Biogeochem. Cycles* **20** GB2017
Aumont O, Ethé C, Tagliabue A, Bopp L and Gehlen M 2015 PISCES-v2: an ocean biogeochemical model for carbon and ecosystem studies *Geosci. Model Dev.* **8** 2465–513
Bach L T, Tamsitt V, Gower J, Hurd C L, Raven J A and Boyd P W 2021 Testing the climate intervention potential of ocean afforestation using the Great Atlantic *Sargassum* Belt *Nat. Commun.* **12** 2556
Berger M, Kwiatkowski L, Ho D T and Bopp L 2023 Ocean dynamics and biological feedbacks limit the potential of macroalgae carbon dioxide removal *Environ. Res. Lett.* **18** 024039
Boucher O *et al* 2020 Presentation and evaluation of the IPSL-CM6A-LR climate model *J. Adv. Model. Earth Syst.* **12** 1–52
Burt D J, Fröb F and Ilyina T 2021 The sensitivity of the marine carbonate system to regional ocean alkalinity enhancement *Front. Clim.* **3** 68
Butenschön M, Lovato T, Masina S, Caserini S and Grosso M 2021 Alkalinization scenarios in the Mediterranean Sea for efficient removal of atmospheric CO_2 and the mitigation of ocean acidification *Front. Clim.* **3** 614537
Duarte C M, Bruhn A and Krause-Jensen D 2022 A seaweed aquaculture imperative to meet global sustainability targets *Nat. Sustain.* **5** 185–93
Dussin R, Barnier B, Brodeau L and Molines J M 2016 *The Making of the Drakkar Forcing Set DFS5* (LGGE)
FAO 2022 The state of world fisheries and aquaculture 2022 (FAO) (available at: www.fao.org/documents/card/en/c/cc0461en)
Feng E Y, Keller D P, Koeve W and Oschlies A 2016 Could artificial ocean alkalinization protect tropical coral ecosystems from ocean acidification? *Environ. Res. Lett.* **11** 074008
Feng E Y, Koeve W, Keller D P and Oschlies A 2017 Model-based assessment of the CO_2 sequestration potential of coastal ocean alkalinization *Earth's Future* **5** 1252–66
Frieder C A *et al* 2022 A macroalgal cultivation modeling system (MACMODS): evaluating the role of physical-biological coupling on nutrients and farm yield frontiers *Mar. Sci.* **9** 752951
Froehlich H E, Afflerbach J C, Frazier M and Halpern B S 2019 Blue growth potential to mitigate climate change through seaweed offsetting *Curr. Biol.* **29** 3087–93.e3
González M F and Ilyina T 2016 Impacts of artificial ocean alkalinization on the carbon cycle and climate in Earth system simulations *Geophys. Res. Lett.* **43** 6493–502
Hauck J, Köhler P, Wolf-Gladrow D and Völker C 2016 Iron fertilisation and century-scale effects of open ocean dissolution of olivine in a simulated CO_2 removal experiment *Environ. Res. Lett.* **11** 024007
He J and Tyka M D 2023 Limits and CO_2 equilibration of near-coast alkalinity enhancement *Biogeosciences* **20** 27–43
Ho D T, Law C S, Smith M J, Schlosser P, Harvey M and Hill P 2006 Measurements of air-sea gas exchange at high wind speeds in the Southern Ocean: implications for global parameterizations *Geophys. Res. Lett.* **33** L16611
Ilyina T, Wolf-Gladrow D, Munhoven G and Heinze C 2013 Assessing the potential of calcium-based artificial ocean

alkalinization to mitigate rising atmospheric CO_2 and ocean acidification *Geophys. Res. Lett.* **40** 5909–14
Jones D C, Ito T, Takano Y and Hsu W-C 2014 Spatial and seasonal variability of the air-sea equilibration timescale of carbon dioxide *Glob. Biogeochem. Cycles* **28** 1163–78
Keller D P, Feng E Y and Oschlies A 2014 Potential climate engineering effectiveness and side effects during a high carbon dioxide-emission scenario *Nat. Commun.* **5** 3304
Keller D P, Lenton A, Scott V, Vaughan N E, Bauer N, Ji D, Jones C D, Kravitz B, Muri H and Zickfeld K 2018 The carbon dioxide removal model intercomparison project (CDRMIP): rationale and experimental protocol for CMIP6 *J. Geophys. Res. Oceans* **11** 1133–60
Kheshgi H S 1995 Sequestering atmospheric carbon dioxide by increasing ocean alkalinity *Energy* **20** 915–22
Köhler P, Abrams J F, Völker C, Hauck J and Wolf-Gladrow D A 2013 Geoengineering impact of open ocean dissolution of olivine on atmospheric CO_2, surface ocean pH and marine biology *Environ. Res. Lett.* **8** 014009
Kwiatkowski L *et al* 2020 Twenty-first century ocean warming, acidification, deoxygenation, and upper-ocean nutrient and primary production decline from CMIP6 model projections *Biogeosciences* **17** 3439–70
Kwiatkowski L, Berger M, Bopp L, Doléac S and Ho D 2023a Contrasting carbon dioxide removal potential and nutrient fedbacks of simulated ocean alkalinity enhancement and macroalgae afforestation *Zenodo* (https://doi.org/10.5281/zenodo.8189997)
Kwiatkowski L, Torres O, Aumont O and Orr J C 2023b Modified future diurnal variability of the global surface ocean CO_2 system *Glob. Change Biol.* **29** 982–97
Lenton A, Matear R J, Keller D P, Scott V and Vaughan N E 2018 Assessing carbon dioxide removal through global and regional ocean alkalinization under high and low emission pathways *Earth Syst. Dyn.* **9** 339–57
Levin L A *et al* 2023 Deep-sea impacts of climate interventions *Science* **379** 978–81
Madec G *et al* 2019 NEMO ocean engine (available at: https://zenodo.org/record/3878122)
Mongin M, Baird M E, Lenton A, Neill C and Akl J 2021 Reversing ocean acidification along the Great Barrier Reef using alkalinity injection *Environ. Res. Lett.* **16** 064068
National Academies of Sciences, Engineering, and Medicine 2022 *A Research Strategy for Ocean-Based Carbon Dioxide Removal and Sequestration* (The National Academies Press) (https://doi.org/10.17226/26278.A)
Orr J C *et al* 2017 Biogeochemical protocols and diagnostics for the CMIP6 Ocean Model Intercomparison Project (OMIP) *Geosci. Model Dev.* **10** 2169–99
Orr J C, Kwiatkowski L and Pörtner H-O 2022 Arctic Ocean annual high in pCO_2 could shift from winter to summer *Nature* **610** 94–100
Orr J C and Sarmiento J L 1992 Potential of marine macroalgae as a sink for CO_2: constraints from a 3D general circulation model of the global ocean *Water Air Soil Pollut.* **64** 405–21
Oschlies A 2009 Impact of atmospheric and terrestrial CO_2 feedbacks on fertilization-induced marine carbon uptake *Biogeosciences* **6** 1603–13
Oschlies A, Koeve W, Rickels W and Rehdanz K 2010 Side effects and accounting aspects of hypothetical large-scale Southern Ocean iron fertilization *Biogeosciences* **7** 4017–35
Paine E R, Boyd P W, Strzepek R F, Ellwood M, Brewer E A, Diaz-Pulido G, Schmid M and Hurd C L 2023 Iron limitation of kelp growth may prevent ocean afforestation *Commun. Biol.* **6** 1–9
Planchat A *et al* 2023 The representation of alkalinity and the carbonate pump from CMIP5 to CMIP6 Earth system models and implications for the carbon cycle *Biogeosciences* **20** 1195–257
Rousset C *et al* 2015 The Louvain-La-Neuve sea ice model LIM3.6: global and regional capabilities *J. Geophys. Res. Oceans* **8** 2991–3005
Séférian R *et al* 2020 Tracking improvement in simulated marine biogeochemistry between CMIP5 and CMIP6 *Curr. Clim. Change Rep.* **6** 95–119
Siegel D A, DeVries T, Doney S C and Bell T 2021 Assessing the sequestration time scales of some ocean-based carbon dioxide reduction strategies *Environ. Res. Lett.* **16** 104003
Smith S *et al* 2023 The state of carbon dioxide removal—1st edition *The State of Carbon Dioxide Removal* (https://doi.org/10.17605/OSF.IO/W3B4Z)
Terhaar J, Orr J C, Gehlen M, Ethé C and Bopp L 2019 Model constraints on the anthropogenic carbon budget of the Arctic Ocean *Biogeosciences* **16** 2343–67
UNCTAD 2022 Review of maritime transport 2022 (Navigating Stormy Waters (UN))
Wang H, Pilcher D J, Kearney K A, Cross J N, Shugart O M, Eisaman M D and Carter B R 2023 Simulated impact of ocean alkalinity enhancement on atmospheric CO_2 removal in the Bering Sea *Earth's Future* **11** e2022EF002816
Wanninkhof R 1992 Relationship between wind speed and gas exchange over the ocean *J. Geophys. Res. Oceans* **97** 7373–82
Wu J, Keller D P and Oschlies A 2023 Carbon dioxide removal via macroalgae open-ocean mariculture and sinking: an Earth system modeling study *Earth Syst. Dyn.* **14** 185–221